LiDAR-Derived High Quality Ground Control Information and DEM for Image Orthorectification

XIAOYE LIU, ZHENYU ZHANG, JIM PETERSON AND SHOBHIT CHANDRA
Center for GIS, School of Geography and Environmental Science, Monash University, Wellington Road, Clayton, VIC 3800, Melbourne, Australia
E-mail: {Xiaoye.Liu, Zhenyu.Zhang, Jim.Peterson, Shobhit.Chandra}@arts.monash.edu.au

Abstract

Orthophotos (or orthoimages if in digital form) have long been recognised as a supplement or alternative to standard maps. The increasing applications of orthoimages require efforts to ensure the accuracy of produced orthoimages. As digital photogrammetry technology has reached a stage of relative maturity and stability, the availability of high quality ground control points (GCPs) and digital elevation models (DEMs) becomes the central issue for successfully implementing an image orthorectification project. Concerns with the impacts of the quality of GCPs and DEMs on the quality of orthoimages inspire researchers to look for more reliable approaches to acquire high quality GCPs and DEMs for orthorectification. Light Detection and Ranging (LiDAR), an emerging technology, offers capability of capturing high density three dimensional points and generating high accuracy DEMs in a fast and cost-effective way. Nowadays, highly developed computer technologies enable rapid processing of huge volumes of LiDAR data. This leads to a great potential to use LiDAR data to get high quality GCPs and DEMs to improve the accuracy of orthoimages. This paper presents methods for utilizing LiDAR intensity images to collect high accuracy ground coordinates of GCPs and for utilizing LiDAR data to generate a high quality DEM for digital photogrammetry and orthorectification processes. A comparative analysis is also presented to assess the performance of proposed methods. The results demonstrated the feasibility of using LiDAR intensity image-based GCPs and the LiDAR-derived DEM to produce high quality orthoimages.

Keywords: orthorectification, orthoimage, LiDAR, LiDAR intensity, DEM

1. Introduction

Advances in computer hardware and software as well as newly emerging technologies, such as sophisticated remote sensing technology and Light Detection and Ranging (LiDAR) systems, have promoted the significant development of traditional spatial mapping procedures. One of the examples is the application of high quality digital orthophotography as a major data source to maintain and update standard maps. Orthophotos, also known as orthoimages if in digital form, are computer-generated images of aerial photographs in which displacements caused by camera or sensor tilts and terrain relief have been removed. As digital orthoimages contains more semantic and visible information than traditional maps, they have great potential of extracting more accurate spatial information for fast updating maps or Geographical Information System (GIS) database.

Quality is essential when using orthoimages in various applications. Errors that affect the quality of orthoimages come from each step of the orthorectification processing. Li *et al* analysed the main factors that affect digital orthoimage accuracy, including aerial photograph scanning, interior orientation, exterior orientation, and differential rectification [32]. As digital photogrammetry technology has reached a stage of relative maturity and stability, the availability of high quality ground control points (GCPs) and digital elevation models (DEMs) becomes the central issue for successfully implementing an image orthorectification project [4], [49]. Concerns with the impacts of the quality of GCPs and DEMs on the quality of orthoimages inspire researchers to look for more reliable approaches to acquire high quality GCPs and DEMs for orthorectification.

Traditionally, the ground control points are obtained either from field survey (including GPS (Global Positioning System) surveying) or by interpretation of existing orthoimages or topographic maps. Although the former method may achieve a higher accuracy for GCPs, it is really time consuming and labour intensive; the drawback of the latter one is the accuracy limitation. Similarly, generating DEMs by field survey or by interpretation of existing topographical maps is neither cost-effective nor reliable. Therefore, specialists in photogrammetry are continuing to look for appropriate approaches to obtaining high quality GCPs and DEMs for image orthorectification processing.

LiDAR, an emerging technology, offers capability of capturing high density and high accuracy three dimensional points in a fast and cost-effective way. One of the appealing features in the LiDAR output is the direct availability of three dimensional coordinates of points in the object space [25]. In addition, most LiDAR systems also have the capability to capture the intensity of the backscattered laser pulse. Although the backscattered LiDAR intensity values are a function of many variables, to some extent, LiDAR intensity data represent the material characteristics of the targets hit by the laser beam. Moreover, LiDAR intensity images have orthogonal geometry characteristics and have high spatial resolution. Ground objects, especially those commonly used for ground controls, such as the intersection of roads and intersection of agricultural plots of land, can be identified from the LiDAR intensity image that corresponds to an aerial image. Therefore, the LiDAR intensity images offer a good alternative of GCPs collection for aerial triangulation calculation in digital photogrammetry. In addition, LiDAR data facilitate the derivation of high accuracy and high resolution DEMs. Our previous research work demonstrated that LiDAR

offers advantages over traditional methods for representing a terrain surface [33], [34]. The advantages refer to accuracy, resolution, and cost. Nowadays, highly developed computer technologies enable rapid processing of huge volumes of LiDAR data, which leads to a great potential to use LiDAR data to get high quality GCPs and DEMs to improve the accuracy of orthoimages.

Rapid maturation of LiDAR technology, continuous falling of prices and increasing accuracy of LiDAR data are causing an exponential availability of LiDAR datasets [25]. However, it is impossible for LiDAR data to replace the traditional remotely sensed imagery because LiDAR data cannot provide as much semantic information as remotely sensed images can. A growing body of research has demonstrated the complementary nature of LiDAR data and traditional remotely sensed data such as aerial photography and mutilspectral or hyperspectral imagery in terms of their geometrical and semantic information [12], [25], [26]. Habib *et al* presented an approach for using linear features derived from LiDAR data into photogrammetric model to align the photogrammetric model relative to the LiDAR reference frame [26]. Their research provided a good alternative for photogrammetric modelling, except for point-based models. Nevertheless, little research has been done for directly using LiDAR's high quality geometric data (particularly, the valuable LiDAR intensity images) for GCPs which are required for aerial triangulation calculation, and for using LiDAR-derived high quality DEMs for orthorectification processing, especially with the utilization of commonly-used point-based commercial digital photogrammetric systems and with no need to develop additional algorithm .

In this article, a concept of four levels of image rectification is proposed, based on current advances in research about image orthorectification. Factors that affect the quality of orthorectified images are analysed, with focus on the GCPs and DEMs. The advantages of using LiDAR data to obtain high quality GCPs and DEMs for orthorectification are addressed. The main part of this paper presents ways for utilizing the LiDAR intensity image for collecting high accuracy GCPs for accurate images orientation to the ground space, and utilizing LiDAR data to derive a high quality DEM for improving planimetric accuracy of digital orthoimages. In addition, a comparative analysis is also presented to assess the performance of proposed methods.

2. Rectification Levels and Quality Issues

2.1. Levels of Image Rectification

Orthorectification is the process of geometrically adjusting a perspective image to an orthogonal image by transforming coordinates from the image space to the ground space and removing tilt and relief displacement. A digital photogrammetric system is usually employed to perform the orthorectification process. A perspective image, camera or sensor calibration information, ground control points and a DEM are the main inputs for orthorectification processing. The final product of orthorectification is a digital orthoimage which combines the image characteristics of a photograph with the geometric quality of a standard map.

The procedure for producing digital orthoimages is well established by using a range of digital photogrammetry systems. It usually includes steps of digital image acquisition, camera or sensor modelling, GCPs collection, aerial triangulation, and image orthorectification. Digital images can be acquired by scanning aerial photography or obtained by using a digital aerial sensor. High spatial resolution

satellite imagery is also an increasingly popular data source for producing orthoimages. Camera/sensor modelling is referred to as interior orientation which defines a camera/sensor's interior geometry as it existed at the time of image capture. Camera calibration information and the measurement of fiducial marks are the primary input for the interior orientation which transforms the image from pixel coordinate system to the image space coordinate system.

In order to define the position and direction orientation of the camera that captured an image, GCPs are required to establish a mathematical relationship between images, camera/sensor, and the ground by using the following collinearity condition equations:

$$x = x_0 - f \cdot \frac{m_{11}(X - X_0) + m_{12}(Y - Y_0) + m_{13}(Z - Z_0)}{m_{31}(X - X_0) + m_{32}(Y - Y_0) + m_{33}(Z - Z_0)}$$

$$y = y_0 - f \cdot \frac{m_{21}(X - X_0) + m_{22}(Y - Y_0) + m_{23}(Z - Z_0)}{m_{31}(X - X_0) + m_{32}(Y - Y_0) + m_{33}(Z - Z_0)}$$

where X_0, Y_0 and Z_0 define the position of the camera station with respect to the ground space coordinate system (*X, Y* and *Z*); x_0 and y_0 are the position of the principal point in the image coordinate system (*x, y*); *f* is the focal length of the camera; and m_{11}, m_{12}, …, and m_{33} are the elements of the rotation matrix. The rotation matrix is derived by applying a sequential rotation of ω about the x-axis, φ about the y-axis, and κ about the z-axis [24]. Once collinearity equations are formulated by using enough ground control and tie points, the least squares adjustment method is used to implement the block triangulation calculation, the results from which are then used as the primary input for the image orthorectification process.

Depending on the input data for the process and the degree of removal of displacement, image rectification usually can be classified as three levels [30], orthorectification being the highest level of the rectification. If nominating raw digital images as the products of level 1, the level 2 rectification processes raw central perspective images with the inputs of orientation parameters and GCPs, but without the information of relief. The resulting product of level 2 processes can be called a 'vertical-image', with tilt displacements being eliminated in the rectified image. The level 3 process adds a further rectification for terrain relief by use of a DEM. On completion of level 3 rectification, the effects of central perspective and displacements due to tilt and terrain relief have been removed so that the resulting image is an orthographic product with a consistent scale. The level 3 rectification is usually referred to as the orthorectification. Recently, the awareness of the concept of 'true orthoimage' in which the displacements due to terrain and buildings or trees are removed is increasingly acknowledged. In the collinearity equations, for a given set of (X, Y, Z), a set of (x, y) should be uniquely resolved, which means that any pixel in the orthoimage has one and only one corresponding pixel in the perspective image. However, in urban or forested area, tall buildings and trees appear oblique and may occlude other objects in the images. As a result, more than one set of (X, Y, Z) points may be projected to the same point (x, y) in the image space. The geometric implication of this many-to-one relationship is referred to as occlusion [45]. In the process of true-orthorectification, a digital surface model (DSM) or a canopy surface model (CSM) or a digital building model (DBM) is employed [8], [45], [56], [57], and the algorithm of removal of occlusion is the core of this process. Here, we nominate this kind of true orthoimage as the product of level 4. The workflow of four levels of rectification with required input data is illustrated in Figure 1.

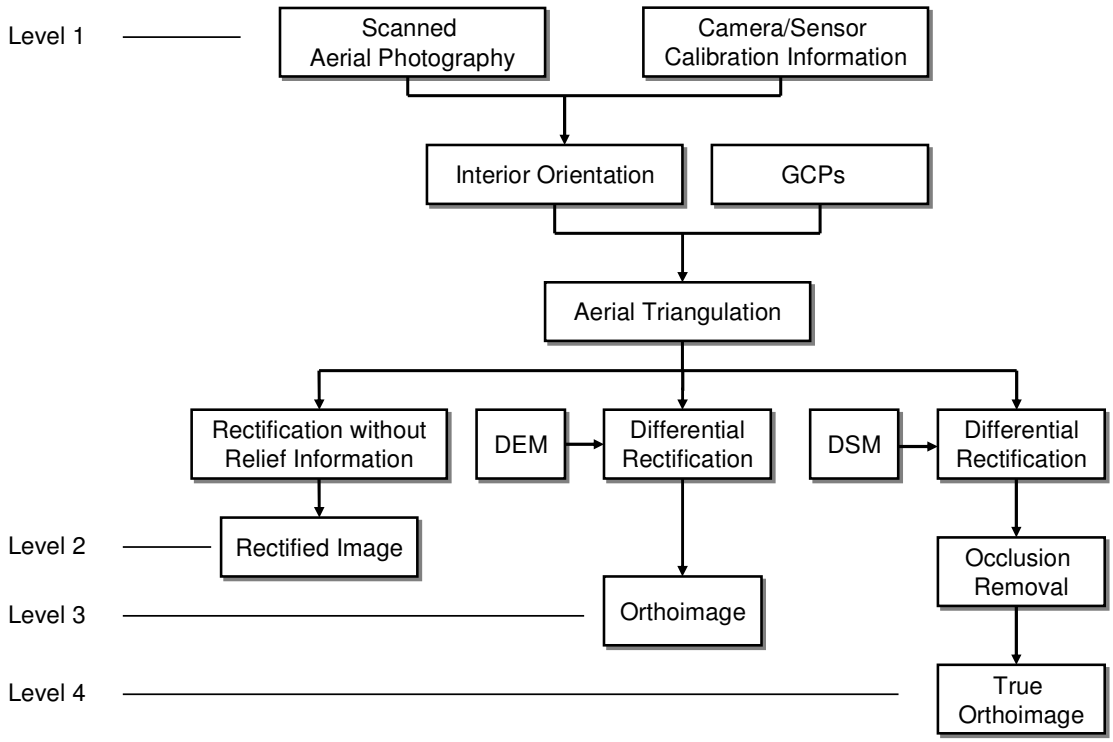

Figure 1. Orthorectification workflow for different levels of products.

The utility of the raw image in practice is limited due to its orthogonal geometric nature and displacements. Objects extracted from level 2 images are more reliable than those from raw images because of their perspective geometric characteristics. In flatter area they have limited relief displacement effects. The most commonly used orthoimages are those from level 3. These perspective images are theoretically free of displacements caused by terrain relief, and have consistent scales. Therefore, features from these images are represented at their correct locations. Distances and angles can be directly measured on level 3 images. For the product of level 4, it has a particular use with large scale of orthoimage in urban or forested areas where displacements caused by buildings or trees could be significant. As the study area of this project is in rural area, the emphasis at this stage is on the process for generating level 3 orthoimags.

2.2. Quality Issues of Image Rectification

Throughout the orthorectification process, a wide range of factors can affect the quality of an orthorectified image [31]. The main scope for error generation exists in the processes of image scanning, interior orientation, exterior orientation, and differential rectification. Image scanning is the process of converting an analogue aerial image to a digital image by using a photogrammetric-quality scanner. The analogue aerial image can be in paper print or film transparency format. Image data can be captured either in reflection modes from paper prints or in transmission mode from film transparencies. Compared to paper prints, film transparencies are the preferred source materials when converting aerial photographs to digital images. Not only are they more dimensionally stable, but also they tend to have higher spatial resolutions and a greater range of grey values [54]. However, paper prints are still the major source materials used for converting to digital images. The accuracy of a converted digital image is mainly dependent on the accuracy of the scanner and the available resolution. For photogrammetric applications, a scanner should be able to scan aerial images (23 x 23 cm) with a minimum optical resolution of 600 dpi, thus providing sufficient radiometric resolution (8 bits with value from 0 - 255 for black and white image or 24 bits - 8 bits for each channel of a colour image) and high geometric accuracy (4 - 12.5 μm minimum pixel size) [10], [11]. The pixel size of scanned aerial images is a function of image scale and scanning resolution selected, and can be calculated by the formula:

$$pixel\_size = \frac{image\_scale}{scanning\_resolution}$$

For example, if scanning an aerial image with a scale of 1:25,.000 by using a scanning resolution of 800 dpi (dots per inch), each pixel in the scanned image will represent

31.25 by 31.25 inches (0.794 by 0.794 m) on the ground. Since every subsequent photogrammetric processing step is based on the scanned imagery, it is important to use a high resolution scanner and select a suitable scanning resolution so that the original image quality can be preserved [32].

The quality of the interior orientation parameters is contingent on the measurement of the photo fiducial marks and the camera calibration information. Therefore, accurate fiducial mark measurement and access to an accurate camera calibration report are crucial if a high quality calculation of interior orientation parameters is to be attained. As far as the quality of exterior orientation parameters and differential rectification is concerned, the quality of GCPs and DEMs is extremely important for the calculation of these two processes. The GCPs and DEMs are the focus of this paper in terms of the analysis of orthoimage quality.

The role of GCPs is to establish an accurate mathematical relationship between the images, the camera/sensor, and the ground so that the exterior orientation parameters of each aerial photograph can be determined. Any inaccuracy of ground control information affects the accuracy of exterior orientation parameters calculated by aerial triangulation, and finally are propagated into the orthorectified images. The absolute accuracy of orthoimages is largely dependent on the quality and the distribution of the GCPs used to orient the image to the ground space [45].

For generation of digital orthoimages from perspective images, a DEM must be used in performing the differential rectification. The role of the DEM is to eliminate the effects of terrain relief displacement. DEM quality is very important to the

orthorectification process because both vertical and horizontal errors in the DEM will be propagated to resulting digital orthoimages, appearing as planimetric (horizontal) errors in the orthoimages. DEM quality becomes more significant to orthorectification process as local relief increases.

3. LiDAR and Potential Advantages of Using LiDAR-Derived GCPs and DEMs

3.1. LiDAR Systems

LiDAR is an active remote sensing technology. It actively transmits pulses of light toward an object of interest, and receives the light that is scattered and reflected by the objects. The distance (range) between the LiDAR sensor and the object can be calculated by multiplying the speed of light by the time it takes for the light to transmit from and return to the sensor [50], [53]. The light used by LiDAR systems varies with applications, depending on the targets to be detected (e.g., their light scattering properties), and the range between the LiDAR sensor and the targets. It could be in the ultraviolet, visible, and near infrared portions of the electromagnetic spectrum [17]. For example, ultraviolet light can be used to detect water vapour in the atmosphere, and near infrared light to detect topographic objects, or ozone, aerosol, and pollutants in the atmosphere [2], [17], [37], [39].

For terrain mapping purpose, an airborne LiDAR system is typically composed of a laser scanner unit, a differential Global Positioning System (dGPS) receiver, and an Inertial Measurement Unit (IMU) [15], [27], [44], [51]. The GPS receiver is used to record the aircraft trajectory at centimetre level and the IMU measures the attitude of the aircraft (roll, pitch, and yaw or heading) [51]. The laser scanner unit consists of a pulse generator of Nd:YAN laser with a wavelength in the range of 0.8 μm to 1.6 μm (typically, with 1.064 μm) and a receiver to get the signal of scattered and reflected

pulses from targets [41], [52]. The laser pulses are typically 10 to 15 ns in duration and have peak energy of several millijoules [2], [52]. Laser pulses are emitted at a rate of 2 kHz to 25 kHz to the Earth surface [3]. The range or distance between the scanner and the target (calculated as stated above) and the position and orientation information obtained from the GPS and IMU to determine target location with high accuracy in three dimensional spaces. The three dimensional points are captured as latitude, longitude, and ellipsoidal height based on the WGS84 reference ellipsoid. They can be transformed to a national or regional coordinate system. At the same time, elevations are converted from ellipsoidal heights to ortho-metric heights based on a national or regional height datum by using a local geoid model [51]. Currently, LiDAR data are typically delivered as tiles in ASCII files containing x, y, z coordinates, and (as clients demand) with LiDAR intensity values.

LiDAR systems are also capable of detecting multiple return signals for a single transmitted pulse [19], [44], [52]. Most LiDAR systems typically record first and last pulse, but some are able to record up to five returns for a single pulse [48]. Multiple returns occur when a laser pulse strike a target that does not completely block the path of the pulse and the remaining portion of the pulse continues on to a lower object. This situation frequently occurs in forested areas where there are some gaps between branches and foliage [44]. Recording multiple returns is quite useful in the description of forest stand and structure. Furthermore, a canopy surface model (CSM) generated by using first returns from the canopy top can be used to generate true orthoimages in forested areas [45].

The raw LiDAR data are three dimensional point clouds. Laser returns are actually recorded from no matter what target the laser beam happens to strike [15], including everything on the ground such as buildings, telephone poles, and power lines. The post-processing of LiDAR data involves the removal of undesirable points and the separation of the bare-earth data from the whole dataset by using filter algorithms [55]. The desired target for DEM generation is the bare-earth. Once the bare-earth points are determined, a high accuracy and high resolution DEM can be generated. The high accuracy and high resolution DEM provides terrain data of high enough quality to refine greatly the elimination of relief displacement during orthorectification.

In addition to the three dimensional coordinates, most LiDAR systems also have the capability to capture the intensity of the backscattered laser pulse. The backscattered laser signal is a function of many variables such as the transmitted laser power, laser beamwidth, range, atmospheric transmission, and effective target cross section (the effective area for collision of the laser beam and the target). The target cross section is strongly dependent on the target reflectance at the laser wavelength, the target area, and the target orientation with respect to the incoming laser beam [20], [28], [43], [48]. The optical signal received by the sensor is converted to an electrical signal by a photodetector (typically an avalanche photodiode). The generated photocurrent or voltage is then quantized to a digital number (usually expressed in percent value, representing the ratio of strength of reflected light to that of emitted light [47]) which is referred to as the LiDAR intensity value for the particular return [14], [20], [28]. The LiDAR intensity data then can be interpolated to a geo-referenced intensity image with orthogonal geometry.

Recently, there have been a few attempts to use LiDAR intensities in glacier monitoring, land cover classification, and forest type identification [9], [13], [36], [40], [47]. However, it should be noted that the backscattered LiDAR intensity values are a function of many other variables in additional to the material characteristics of the targets hit by the laser beam. Furthermore, unlike aerial photography or multispectral satellite imagery, LiDAR intensity data contain information about objects' reflectance at only a specific wavelength (e.g., 1.064 μm). All of these factors will adversely influence the application of LiDAR intensity data (especially for the application of intensity data for land cover classification) unless the LiDAR intensity data have been radiometrically calibrated [20], [27], [29], [42], [43].

In this project, however, since the LiDAR data have high spatial resolution, many ground objects, especially those commonly used for ground controls such as the intersection of roads and intersection of agricultural plots of land can be easily recognized from LiDAR intensity images. In addition, LiDAR intensity images have orthogonal characteristics. Therefore, it should be possible to directly collect higher accuracy ground coordinates of GCPs from intensity images for digital photogrammetric process.

Airborne LiDAR is still a rapidly growing technology. An important development is the integration of a high resolution digital camera or a digital video camera with a LiDAR system [3], [5]. For each collected digital image, the position and orientation of the camera can be obtained by using the GPS and IMU data. Exterior orientation parameters for each frame of imagery are directly provided by these position and orientation data. Therefore, no stereo overlapping images and/or ground control points are needed. Orthorectification can be completely automatic by using the digital

images and a LiDAR-derived DEM [5]. It is expected that the LiDAR system can be combined with multispectral or hyperspectral imaging systems, which will result in highly versatile systems and extended LiDAR application potential [3].

3.2. Potential Advantages of Using LiDAR-Derived GCPs and DEMs

The availability of increasingly sophisticated and automated digital image processing systems has facilitated the use of photogrammetric techniques in a wide range of applications [13]. However, the quality of GCPs and DEMs has been a big concern in the production of digital orthoimages. The availability of high accuracy GCPs and DEMs becomes the key issue for successful implementation of an image orthorectification project.

As stated in section 1, traditionally, GCPs can be collected from field survey (using total station or GPS), topographic maps, and national or state spatial infrastructure data. All these methods are either time consuming and labour intensive or lack of enough accuracy. In practice, in order to increase the redundancy that is beneficial for gross error detection, and to prepare independent GCPs check points, it is quite common to use more GCPs than minium number of GCPs required for the block triangulation. Moreover, to ensure the calculation quality, GCPs should be evenly distributed over the image covered area. It is a very difficult task for collecting a large number of high quality GCPs by using traditional methods to meet all the aforementioned requirements for digital photogrammetric and orthorectification process.

DEMs are commonly generated from such datasets as topographic maps, stereo aerial photography, satellite imagery or field survey. The drawbacks of using these kinds of

ways for DEM generation are either their limitations of accuracy or their labour intensity. Fortunately, LiDAR offers the capability of capturing high density points and high accuracy digital elevation data in a fast and cost-effective way. It has great potential to provide high quality of GCPs and DEMs for orthorectification process requirements.

There are significant advantages of using LiDAR data to provide GCPs and DEMs for orthorectification process. First, the increasing availability of LiDAR data makes it possible to provide high accuracy three dimensional points with high density and even distribution over large areas. Second, due to its high accuracy and high visual interpretable nature of intensity image, high quality GCPs can be directly picked up from this image. Third, with high resolution and high accuracy LiDAR-derived DEMs, it is possible to remove relief displacement at complicated terrain conditions. Finally, LiDAR enables rapid acquisition of three dimensional points and intensity over large areas so that the labour expenditure and other costs can be reduced since time is money. However, it should be noted that the LiDAR market is not stable because the LiDAR technology is in a development stage [12]. The cost of LiDAR data acquisition can vary, depending on size of project, point density, and project location. It is evident that, using LiDAR to collect data and generate DEM is a cost effective way, comparing with field survey (using total station or GPS), especially over a large area. Therefore, it is no doubt an economical way for GCPs collection by using LiDAR intensity data which is a by-product of a LiDAR terrain mapping project.

4. Study Area, Data and Method

4.1. Study Area

The study area is in the region of Corangamite Catchment Management Authority (CCMA), which is located in the south western Victoria, Australia. The landscape in the region can be depicted to north and south highlands and a large Victoria Volcanic Plain (VVP) in the middle. LiDAR data for the total area of 6900 km², covering most part of VVP in the CCMA, were collected over the period of 19 July 2003 to 10 August 2003. These areas have high priority for a range of research projects pertaining to environment management issues addressed in the catchment management strategy plan. The primary purpose of these LiDAR data is to accurately represent terrain pattern in this area, and combining with aerial photography, satellite imagery, and other spatial data, to implement a serious of environment related projects.

4.2. Data

The estimate of accuracy of LiDAR data used for this project is documented as 0.5 metres for vertical accuracy and 1.5 metres for horizontal accuracy [1]. LiDAR data were first classified into bare-earth and non-ground points using different algorithms across the project area [1]. Manual checking and editing of the data were also conducted to further improve the quality of the classification [1]. The bare-earth LiDAR points were used to generate a grid DEM.

Interpolation methods available for constructing a DEM from sample elevation points can be classified: deterministic methods such as inverse distance weighted (IDW) (assumes that each input point has a local influence that diminishes with distance) and spline-based methods that fit a minimum-curvature surface through the sample points; and geostatistical methods such as Kriging that takes into account both the distance and the degree of autocorrelation (the statistical relationship among the sample points).

New or modified interpolation methods are still being developed [7], [46]. To evaluate the performance of some commonly-used interpolation methods, several comparisons of these interpolators have been conducted for different practical purposes [6], [16], [18], [35], [38], [58]. None of the interpolation methods is universal for all kinds of data sources, terrain patterns, or purposes. However, if sampling data density is high, the IDW method performs well, even for complex terrain [6], [16], [18]. LiDAR data have high sampling density, and so the IDW approach was selected as the interpolator for our LiDAR data processing. Using ArcGIS software, a regular 5 by 5 meters grid DEM and a DSM were created by using the elevation values of the bare-earth points and all the points separately. Meanwhile, LiDAR intensity data were also interpolated into a raster image with the spatial resolution of one metre by using all the LiDAR points.

Natural colour aerial photography was collected in April 2000 at a nominal height of 3825 m above ground level and a scale of 1:25,000. A high resolution scanner was used to convert these film-based aerial photos to digital images. The resulting images have a 0.8 m spatial resolution.

GPS surveys were conducted in the study area in November 2005 and May 2006. A total of 50 GPS points were used in this study to assess the planimetric accuracy of the LiDAR intensity image. By comparing the coordinates of GPS points with those of the corresponding locations from LiDAR intensity image, the results show that the maximum position difference is 1.10 m, minimum 0.36 m, average 0.69m, and the RMSE is 0.56 m. Therefore, the LiDAR intensity images proved to be of high accuracy.

In order to assess the performance of proposed methodologies, especially to compare with commonly used ground control data and DEMs for orthorectification, some of the *Vicmap* datasets including *Vicmap Elevation*, *Vicmap Transport*, and *Vicmap Features* datasets are also gathered. *Vicmap* is a set of spatially related data products made up from individual datasets. They provide foundation to Victorian primary mapping and geographic information systems. All these datasets are produced and maintained by the Victorian Department of Sustainability and Environment, Australia.

Vicmap Elevation, a statewide 20 m resolution DEM which is structured in a regular array of pixels representing Victoria's terrain surface, is a commonly used elevation data source in Victoria for various terrain-related applications and processes including orthorectification. *Vicmap DEM* was produced by using elevation data mainly derived from existing 1:25,000 contour maps and digital stereo capture. Estimated standard deviations are 5m and 10m for vertical and horizontal accuracy respectively [21].

Vicmap Transport models transport infrastructure networks for Victoria. Primary feature types in *Vicmap Transport* are road centrelines and railways. *Vicmap Features* contains infrastructure features such as fence lines, utility lines and landmarks. From the perspective of digital photogrammetric processing, road centrelines and fence lines are the most interesting features for collecting GCPs. However, the accuracy of these datasets should be noted when using them for the purpose of GCP collection. The estimated standard deviation for these features is 8.2 m [22], [23]. It may be not suitable for GCP collection for large scale aerial image orthorectification.

4.3. Method

Erdas Imagine 8.7 (a digital photogrammetric software package) is used to process digital images from scanned aerial photographs. An example of these images used for this study is shown in Figure 2. Features depicted include agricultural lands, residential areas, roads, trees, and salt lakes. These raw digital perspective images are the original input images to undergo block triangulation and orthorectification. The subsequent steps are to enter the camera calibration data, measure the fiducial marks on the images, and perform interior orientation parameters calculation for each image.

Figure 2. An example of scanned natural colour aerial photographs with highlighted positions of GCPs measurements.

Following the interior orientation, it is ready to measure the positions of GCPs in the images and provide their correspondent ground (or object space) coordinates for aerial triangulation. The LiDAR intensity image has an orthogonal nature and is georeferenced to the Geocentric Datum of Australia 94 (GDA94) and projected to the

MGA Zone 54 coordinate system so that it is much like a high accuracy large scale topographic map. The LiDAR intensity image makes it much easier to identify features such as road intersections and agricultural land plot boundaries, which are commonly used as GCPs. Due to the high accuracy characteristics of LiDAR data, the intensity image is well suited for providing ground control truth information for aerial triangulation calculation. Therefore, the X and Y coordinates of GCPs in object space can be directly collected from LiDAR intensity images; Z coordinates being obtained from the LiDAR-derived DEM. An example of LiDAR intensity images used for this study is shown in Figure 3, which covers the same area as the aerial image in Figure 2. Highlighted marks represent the locations where the ground coordinates of GCPs were picked up.

Figure 3. A LiDAR intensity image, which covers the same area as the scanned aerial photograph in Figure 2.

Once the aerial triangulation process is complete, digital orthorectification can be conducted. During this process, the raw digital imagery is resampled to the correct ground position. The effects of terrain relief displacement are removed by utilizing a LiDAR-derived high quality DEM.

With the aim of assessing the suitability of using GCPs derived from the LiDAR intensity image for aerial triangulation and of using the LiDAR-derived DEM for image orthorectification, the scanned aerial images same as above but using *Vicmap* data for providing GCPs and DEM were input to the same digital photogrammetric software for aerial triangulation and orthorectification. Here, the object space coordinates of GCPs were obtained from *Vicmap Transport* and *Vicmap Features*. The DEM was based on 20 m resolution *Vicmap Elevation* data. For the purpose of comparison, the same object features were used for GCPs and the same number of GCPs was picked up.

5. Results and discussion

Using the method described above, scanned natural colour aerial photographs were orthorectified to the final orthoimages. GCPs and the DEM used for the photogrammetric and orthorectification process were obtained from LiDAR data and *Vicmap* data separately. An example of the orthorectified image by using LiDAR-generated GCPs and DEM, draped on a LiDAR-derived digital surface model (DSM) is shown in Figure. 4. The features on this orthoimage should be in their correct positions. The reference LiDAR intensity image draped on terrain surface, covering same area as in Figure 4 is shown in Figure 5.

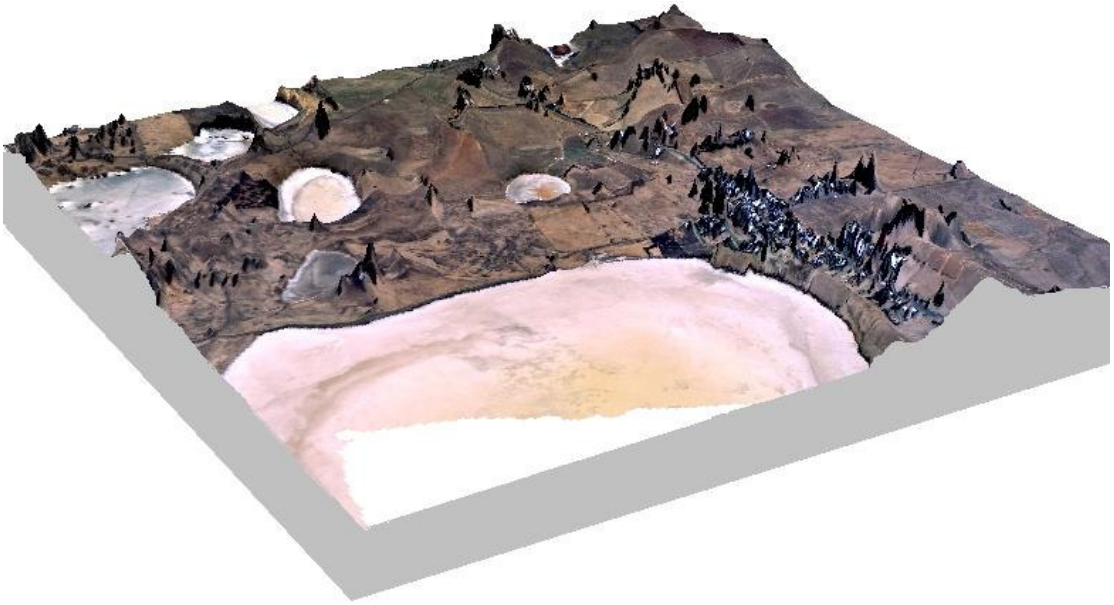

Figure 4. 3D visualization of an orthorectified aerial photograph depicting part of the study area.

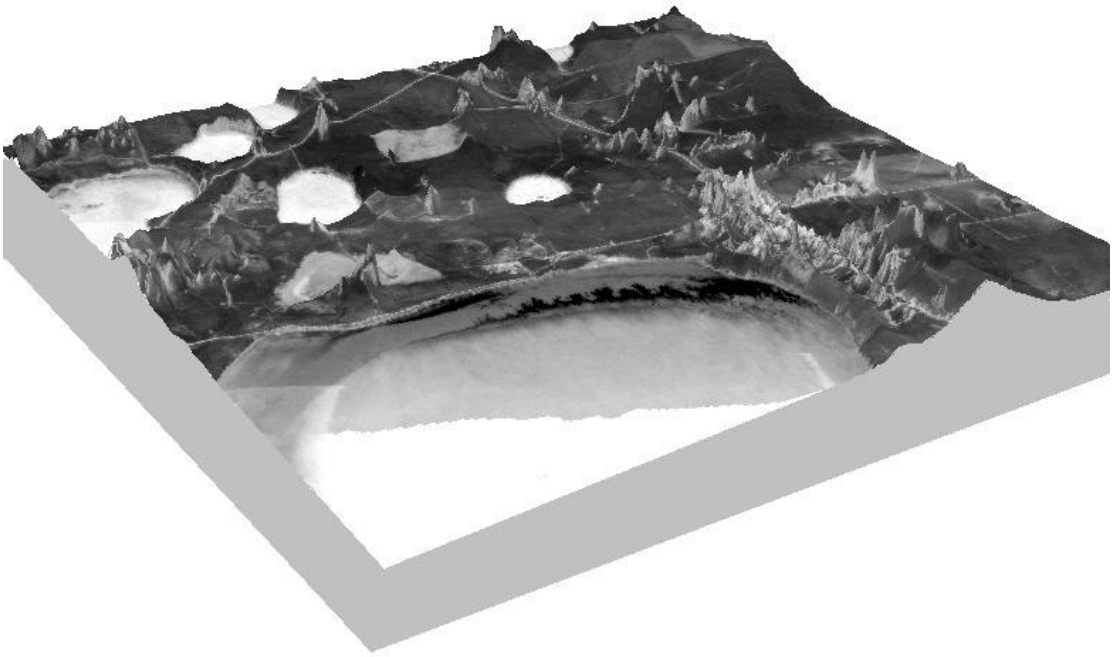

Figure 5. 3D visualization of the LiDAR intensity image covering same area as depicted in Figure. 4.

The purpose of this project is to investigate the feasibility of using LiDAR data to implement image orthorectification for improving the accuracy of orthorectified images. It is necessary to use some quality indicators to assess the accuracy of the

resulting orthoimages. For orthoimages, it is important to evaluate the planimetric accuracy. The X and Y coordinates of check points in the orthoimage were measured, and then compared with the corresponding coordinates from differential GPS surveys. The planimetric position differences between orthoimages (orthorectified based on LiDAR data on the one hand and *Vicmap* data on the other) and the GPS check points are listed in Table 1. Based on these data, a statistic diagram was drawn in Figure. 6, showing position differences of each check points for the image orthorectified using LiDAR data, and for the image orthorectified using *Vicmap* data.

Table 1. Planimetric position accuracy.

Coordinates from GPS Survey (I_0) (m)		Coordinates from LiDAR-orthorectified Image (I_1) (m)		Coordinates from Vicmap-orthorectified Image (I_2) (m)		Position Difference (m)	
X	Y	X	Y	X	Y	$\|I_1 - I_0\|$	$\|I_2 - I_0\|$
31761.84	67258.49	31762.11	67258.18	31759.93	67262.49	0.41	4.43
28414.79	69458.39	28415.61	69459.89	28408.02	69451.09	1.70	9.96
31037.51	68701.59	31037.87	68702.45	31036.01	68697.75	0.93	4.12
30929.38	68945.13	30929.68	68945.75	30929.75	68941.39	0.69	3.76
30811.17	69179.83	30811.37	69179.08	30809.47	69173.26	0.78	6.78
30946.31	69179.32	30946.86	69180.80	30944.89	69174.17	1.58	5.34
31079.91	69164.53	31079.79	69165.92	31078.41	69160.95	1.40	3.88
31058.73	68933.38	31058.82	68934.54	31057.69	68929.27	1.16	4.24
26961.03	67486.52	26961.47	67486.66	26957.27	67482.76	0.46	5.32
28207.44	68641.17	28207.27	68641.34	28200.98	68639.31	0.24	6.71
29092.21	71499.51	29091.44	71500.97	29080.72	71498.04	1.65	11.58
30845.77	69443.33	30846.16	69445.14	30852.78	69437.85	1.85	8.90
31114.13	70633.01	31114.04	70631.52	31110.87	70629.64	1.49	4.69
31029.86	70956.87	31030.13	70955.69	31027.14	70954.58	1.21	3.56
31152.02	68461.31	31152.28	68462.69	31151.08	68457.58	1.40	3.85
30147.19	72033.51	30147.43	72031.94	30136.48	72035.53	1.59	10.90
31026.37	68469.42	31026.81	68469.96	31025.49	68465.69	0.70	3.83
31211.47	69158.06	31212.29	69156.86	31209.59	69148.07	1.45	10.17
28396.05	70296.71	28396.59	70295.53	28389.80	70287.15	1.30	11.42
25757.33	67071.38	25756.67	67072.75	25756.05	67063.85	1.52	7.64

Table 1 and Figure 6 clearly indicate that the orthorectified image by using LiDAR-derived GCPs and the LiDAR DEM has much higher planimetric position accuracy than that by using *Vicmap* based data. The maximum position difference in the LiDAR-orthorectified image is 1.85 m, while the difference is up to 11.58 m in

Vicmap-orthorectified image. By using the following formula, the root mean square errors (RMSE) were calculated as 1.30 m for LiDAR-orthorectified orthoimage and 7.26 m for *Vicmap*-orthorectified orthoimage

$$\sigma_P = \sqrt{\frac{\sum \Delta P^2}{n-1}}$$

where, ΔP is the calculated position difference between the orthoimage and GPS survey, and n is the total number of points.

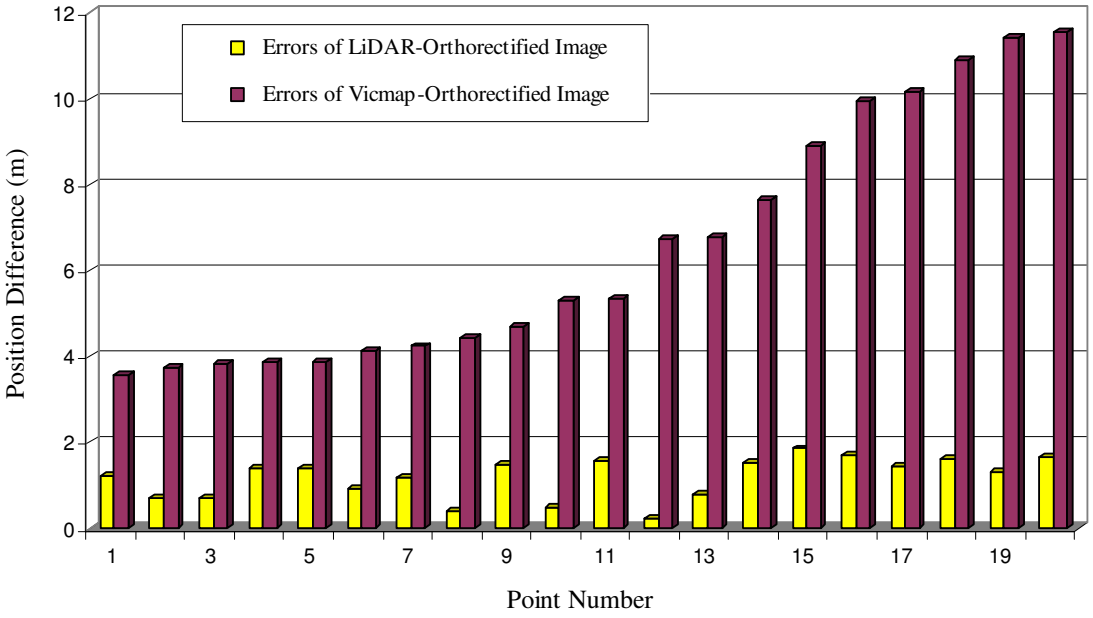

Figure 6. Planimetric position accuracy

The planimetric position accuracy of an orthoimage is a function of the quality of the input GCPs, DEM, and also some other factors. The accuracy of GCPs and the DEM is reflected in the accuracy of the orthoimage. The experiment results demonstrated that the competent use of LiDAR-based GCPs and LiDAR-derived DEM can ensure high quality for orthorectification. Given the accuracy of LiDAR data used for this

project, a high accuracy of horizontal position for orthorectified images can certainly be achieved. GCP coordinates acquired from LiDAR intensity image and the DEM generated from LiDAR data are well suited for the orthorectification process of aerial photography of medium and large scales.

LiDAR data do not only provide high accuracy GCPs and DEM for improving the accuracy of an orthorectified image, they but also have great potential to reduce the costs of orthorectification of aerial photography, especially for remote areas. With the increasing availability and steadily decreasing cost of LiDAR data, it is becoming common for remotely sensed overlaying datasets to include not only aerial photography but LiDAR data also. It has attracted an increasing amount of interest to explore these data's complementary characteristics. The results lead to the potential decrease of the costs of a specific traditional process, such as using LiDAR data to support the orthorectification of aerial photography.

6. Conclusion

Different levels of image rectification and factors contributing to orthorectified images were first addressed in this paper. Then it presented a way of using LiDAR-derived GCPs and DEMs for image orthorectification. High accuracy LiDAR data offer the capability of obtaining GCPs and DEMs at a higher level of accuracy required for photogrammetric and orthorectification processes. The ground coordinates of GCPs were obtained from LiDAR intensity map, while DEMs were generated from high accuracy 3D LiDAR point clouds. The experiment results in this paper demonstrated the practical feasibility of taking advantage of LiDAR based GCPs and LiDAR-derived DEM in digital photogrammetry to produce high quality orthorectified images. The orthoimage accuracy by using LiDAR data is superior to

that achieved by using lower accuracy data sources such as *Vicmap*. In addition to the accuracy aspect, it is expected that using LiDAR data for orthorectification process would be a cost effective way. This is especially true with the increasing availability of LiDAR data and the expected drop in costs.

Acknowledgment

The authors would like to thank three anonymous reviewers for their valuable comments and suggestions. We are also grateful to the Corangamite Catchment Management Authority for providing LiDAR data and other datasets to support this project.

References

1. AAMHatch. Corangamite CMA airborne laser survey data documentation, AAMHatch Pty Ltd, Melbourne, Australia, 2003.
2. Y. B. Acharya, S. Sharma and H. Chandra. "Signal induced noise in PMT detection of lidar signals", *Measurement*, Vol. 35(3):269-276, 2004.
3. F. Ackermann. "Airborne laser scanning - present status and future expectations", *ISPRS Journal of Photogrammetry and Remote Sensing*, Vol. 54(4):64-67, 1999.
4. F. Ackermann and P. Krzystek. "Complete automation of digital aerial triangulation", *Photogrammetric Record*, Vol. 15(89):645-656, 1997.
5. S. Ahlberg, U. Söderman, M. Elmqvist and A. Persson. "On modelling and visualisation of high resolution virtual environments using lidar data", in *Proceedings of 12th International Conference on Geoinformatics*, Gävle, Sweden, 2004. pp.299-306.

6. T. A. Ali. "On the selection of an interpolation method for creating a terrain model (TM) from LIDAR data", in *Proceeding of the American Congress on Surveying and Mapping (ACSM) Conference 2004*, Nashville TN, U.S.A, 2004.

7. A. Almansa, F. Cao, Y. Gousseau and B. Rougé. "Interpolation of digital elevation models using amle and related methods", *IEEE Transactions on Geoscience and Remote Sensing*, Vol. 40(2):314-325, 2002.

8. F. Amhar, J. Jansa and C. Ries. "The generation of true orthophotos using a 3D building model in conjunction with a conventional DTM", *International Archives of the Photogrammetry, Remote Sensing and Spatial Information Sciences*, Vol. 32(Part 4):16-22, 1998.

9. N. S. Arnold, W. G. Rees, B. J. Devereux and G. S. Amable. "Evaluating the potential of high-resolution airborne LiDAR data in glaciology", *International Journal of Remote Sensing*, Vol. 27(6):1233-1251, 2006.

10. E. Baltsavias and R. Bill. "Scanners - a survey of current technology and future needs ", *International Archives of the Photogrammetry, Remote Sensing and Spatial Information Sciences*, Vol. 30(Part 1):130-143, 1994.

11. E. P. Baltsavias. "Photogrammetric scanners - survey, technological developments and requirements", *International Archives of the Photogrammetry, Remote Sensing and Spatial Information Sciences*, Vol. 32(Part 1):44-52, 1998.

12. E. P. Baltsavias. "A comparison between photogrammetry and laser scanning", *ISPRS Journal of Photogrammetry and Remote Sensing*, Vol. 54(4):83-89, 1999.

13. E. P. Baltsavias, E. Favey, A. Bauder and H. Bosch. "Digital surface modelling by airborne laser scanning and digital photogrammetry for glacier monitoring", *Photogrammetric Record*, Vol. 17(98):243-273, 2001.

14. M. Barbarella, V. Lenzi and M. Zanni. "Integration of airborne laser data and high resolution satellite images over landslides risk areas", *International Archives of the Photogrammetry, Remote Sensing and Spatial Information Sciences*, Vol. 35(B4):945-950, 2004.

15. C. P. Barber and A. M. Shortrudge. Light Detection and Ranging (LiDAR)-derived elevation data for surface hydrology applications, Institute of Water Resource, Michigan State University, USA, 2004.

16. T. Blaschke, D. Tiede and M. Heurich. "3D landscape metrics to modelling forest structure and diversity based on laser scanning data", *International Archives of the Photogrammetry, Remote Sensing and Spatial Information Sciences*, Vol. 36(8/W2):129-132, 2004.

17. E. V. Browell, W. B. Grant and S. Ismail. "Airborne LiDAR system", in T. Fujii and T. Fukuchi (Eds.), *Laser Remote Sensing*, Taylor & Francis: Boca Raton, London, New York and Singapore, pp. 723-779, 2005.

18. V. Chaplot, F. Darboux, H. Bourennane, S. Leguédois, N. Silvera and K. Phachomphon. "Accuracy of interpolation techniques for the derivation of digital elevation models in relation to landform types and data density", *Geomorphology*, Vol. 77(1-2):126-141, 2006.

19. A. P. Charaniya, R. Manduchi and S. K. Lodha. "Supervised parametric classification of aerial LiDAR data ", in *Proceedings of 2004 Conference on Computer Vision and Pattern Recognition Workshop (CVPRW'04)*, Washington D.C, USA, 2004.

20. F. Coren, D. Visintini, G. Prearo and P. Sterzai. "Integrating LiDAR intensity measures and hyperspectral data for extracting of cultural heritage", in *Proceedings of Italy - Canada 2005 Workshop on 3D Digital Imaging and Modeling: Applications of Heritage, Industry, Medicine and Land*, Padova, Italy, 2005.

21. DSE. Product Description - Vicmap Elevation, Department of Sustainability and Environment, Victoria, Australia, 2002.

22. DSE. Product Description - Vicmap Features, Department of Sustainability and Environment, Victoria, Australia, 2005.

23. DSE. Product Description - Vicmap Transport, Department of Sustainability and Environment, Victoria, Australia, 2005.

24. Leica Geosystems. Leica photogrammetry suite orthoBASE & orthoBASE Pro user's guide, Leica Geosystems GIS & Mapping, LLC, Atlanta, Georgia, USA, 2003.

25. A. Habib, M. Ghanma, M. Morgan and R. Al-Ruzouq. "Photogrammetric and LiDAR data registration using linear features", *Photogrammetric Engineering and Remote Sensing*, Vol. 71(6):699-707, 2005.

26. A. F. Habib, M. S. Ghanma, C. J. Kim and E. Mitishita. "Alternative approaches for utilizing LiDAR as a source of control information for photogrammetric models", *International Archives of the Photogrammetry, Remote Sensing and Spatial Information Sciences*, Vol. 35(B1):193-198, 2004.

27. M. Hollaus, W. Wagner and K. Kraus. "Airborne laser scanning and usefulness for hydrological models", *Advances in Geosciences*, Vol. 5(1):57-63, 2005.

28. A. V. Jelalian. Laser Radar Systems, Artech House: Boston and London, 1992.

29. S. Kaasalainen, E. Ahokas, J. Hyyppä and J. Suomalainen. "Study of surface brightness from backscattered laser intensity: calibration of laser data", *IEEE Geoscience and Remote Sensing Letters*, Vol. 2(3):255-259, 2005.

30. M. Kasser and Y. Egels. Digital Photogrammetry, Taylor and Francis: London and New York, 2002.

31. A. Krupnik. "Accuracy prediction for ortho-image generation", *Photogrammetric Record*, Vol. 18(101):41-58, 2003.

32. D. Li, J. Gong, Y. Guan and C. Zhang. "Accuracy analysis of digital orthophotos", *International Archives of the Photogrammetry, Remote Sensing and Spatial Information Sciences*, Vol. 36(W20):241-244, 2002.

33. X. Liu, J. Peterson and Z. Zhang. "High-resolution DEM generated from LiDAR data for water resource management", in *Proceedings of International Congress on Modelling and Simulation 'MODSIM05'*, Melbourne, Australia, 2005. pp.1402-1408.

34. X. Liu, J. Peterson, Z. Zhang and S. Chandra. "Improving soil salinity prediction with high resolution DEM derived from LiDAR data", *International Archives of the Photogrammetry, Remote Sensing and Spatial Information Sciences*, Vol. 36(7/W20):41-43, 2005.

35. C. D. Lloyd and P. M. Atkinson. "Deriving ground surface digital elevation models from LiDAR data with geostatistics", *International Journal of Geographical Information Science*, Vol. 20(5):535-563, 2006.

36. J. L. Lovell, D. L. B. Jupp, D. S. Culvenor and N. C. Coops. "Using airborne and ground-based ranging lidar to measure canopy structure in Australian forests", *Canadian Journal of Remote Sensing*, Vol. 29(5):606-622, 2003.

37. A. Macke and M. Groβklaus. "Light scattering by nospherical raindrops: implications for LiDAR remote sensing of rainrates ", *Journal of Quantitative Spectroscopy & Radiative Transfer*, Vol. 60(3):355-363, 1998.

38. M. G. Mardikis, D. P. Kalivas and V. J. Kollias. "Comparison of interpolation methods for the prediction of reference evapotranspiration - an application in Greece", *Water Resources Management*, Vol. 19(3):251-278, 2005.

39. G. Méjean, J. Kasparian, E. Salmon, J. Yu, J. P. Wolf, R. Bourayou, R. Sauerbrey, M. Rodriguez, L. Wöste, H. Lehmann, B. Stecklum, U. Laux, J. Eislöffel, A. Scholz and A. P. Hatzes. "Towards a supercontinuum-based infrared lidar", *Applied Physics B: Lasers and Optics*, Vol. 77(2-3):357-359, 2003.

40. T. Moffiet, K. Mengersen, C. Witte, R. King and R. Denham. "Airborne laser scanning: exploratory data analysis indicates potential variables for classification of individual trees or forest stands according to species", *ISPRS Journal of Photogrammetry and Remote Sensing*, Vol. 59(5):289-309, 2005.

41. T. Mukai, A. M. Nakamura and T. Sakai. "Asteroidal surface studies by laboratory light scattering and LIDAR on HAYABUSA", *Advances in Space Research*, Vol. 37(1):138-141, 2006.

42. J. A. Parian and A. Gruen. "Integrated laser scanner and intensity image calibration and accuracy assessment", *International Archives of the Photogrammetry, Remote Sensing and Spatial Information Sciences*, Vol. 36(3/W19):18-23, 2005.

43. C. E. Parrish, G. H. Tuell, W. E. Carter and R. L. Shrestha. "Configuring an airborne laser scanner for detecting airport obstructions", *Photogrammetric Engineering and Remote Sensing*, Vol. 71(1):37-46, 2005.

44. S. E. Reutebuch, H. E. Andersen and R. J. McGaughey. "Light detection and ranging (LIDAR): an emerging tool for multiple resource inventory", *Journal of Forestry*, Vol. 103(6):286-292, 2005.

45. Y. Sheng, P. Gong and G. S. Biging. "Orthoimage production for forested areas from large-scale aerial photographs", *Photogrammetric Engineering and Remote Sensing*, Vol. 69(3):259-266, 2003.

46. W. Z. Shi and Y. Tian. "A hybrid interpolation method for the refinement of a regular grid digital elevation model", *International Journal of Geographical Information Science*, Vol. 20(1):53-67, 2006.

47. J. H. Song, S. H. Han, K. Yu and Y. I. Kim. "Assessing the possibility of land-cover classification using lidar intensity data", *International Archives of the Photogrammetry, Remote Sensing and Spatial Information Sciences*, Vol. 34(Part 3A):259-262, 2002.

48. W. Wagner, A. Ullrich, T. Melzer, C. Briese and K. Kraus. "From single-pulse to full-waveform airborne laser scanners: potential and practical challenges", *International Archives of the Photogrammetry, Remote Sensing and Spatial Information Sciences*, Vol. 35(B3), 2004.

49. A. S. Walker. "Responses to users: the continuing evolution of commercial digital photogrammetry", *Photogrammetric Record*, Vol. 16(93):469-483, 1999.

50. D. Watkins. LiDAR types and uses: with a case study in forestry, Department of Geography, Pennsylvania State University, USA, 2005.

51. T. L. Webster and G. Dias. "An automated GIS procedure for comparing GPS and proximal LiDAR elevations", *Computers & Geosciences*, Vol. 32(6):713-726, 2006.

52. A. Wehr and U. Lohr. "Airborne laser scanning - an introduction and overview ", *ISPRS Journal of Photogrammetry and Remote Sensing*, Vol. 54(4):68-82, 1999.

53. C. Weitkamp. "LiDAR: Introduction", in T. Fujii and T. Fukuchi (Eds.), *Laser Remote Sensing*, Taylor & Francis: Boca Raton, London, New York and Singapore, pp. 1-36, 2005.

54. R. Welch and T. Jordan. "Using scanned aerial photographs", in S. Morain and S. L. Baros (Eds.), *Raster Imagery in Geographic Information Systems*, OnWord Press: Santa Fe, NM, USA, pp. 55-69, 1996.

55. K. Q. Zhang, S. C. Chen, D. Whitman, M. L. Shyu, J. H. Yan and C. C. Zhang. "A progressive morphological filter for removing nonground measearements from airborne LiDAR data", *IEEE Transactions on Geoscience and Remote Sensing*, Vol. 41(4):872-882, 2003.

56. G. Zhou, W. Chen, J. A. kelmelis and D. Zhang. "A comprehensive study on urban true orthorectification", *IEEE Transactions on Geoscience and Remote Sensing*, Vol. 43(9):3138-2147, 2005.

57. G. Zhou, W. Schichler, A. Thorpe, P. Song, W. Chen and C. Song. "True orthoimage generation in urban areas with very tall buildings", *International Journal of Remote Sensing*, Vol. 25(22):5163-5180, 2004.

58. D. Zimmerman, C. Pavlik, A. Ruggles and M. P. Armstrong. "An experimental comparison of ordinary and universal Kriging and inverse distance weighting", *Mathematical Geology*, Vol. 31(4):375-389, 1999.